Role of 2×1 domain boundaries on the transition from 2×1 to $c(2\times8)$ at Ge(111) surfaces

Y. Einaga, H. Hirayama,* and K. Takayanagi
Department of Materials Science and Engineering, Interdisciplinary Graduate School of Science and Engineering, Tokyo Institute of Technology, 4259 Nagatsuda, Yokohama 226, Japan
(Received 14 January 1998)

We studied the role of 2×1 domain boundaries and steps on the irreversible transition from 2×1 to $c(2\times8)$ reconstruction at the Ge(111) surface. The as cleaved Ge(111) surface reconstructs to a 2×1 structure with two types of domain boundaries and steps. The π-bonded chains rotate by 120° at the type-*A* boundary, whereas the π-bonded chains are parallel but stagger by a half-unit cell at the type-*B* boundary. The bilayer-height step is also classified into a type-*A* step, to which π-bonded chains make an angle of 120°, and a type-*B* step, to which π-bonded chains are parallel. In annealing, we found that the 2×1 reconstruction was first disordered, and then changed to a $c(2\times8)$ reconstruction. The disordered area included adatoms, arranged with $c(2\times4)$ and 2×2 short-range ordering, and holes. We observed that this disordering began preferentially from the type-*A* boundary and type-*A* step of the 2×1 domain above 120 °C. In contrast, the type-*B* boundary and type-*B* step were stable against disordering. In a detailed analysis of scanning tunneling microscopy images, we proposed an atomic structure model of a type-*B* boundary in which staggered π-bonded chains were smoothly bridged with no additional dangling bonds. However, smooth bridging was impossible at the type-*A* boundary, and the edge atoms at this boundary were unstable. The type-*A* boundary and type-*A* step, therefore, can release additional adatoms. This created holes at the boundary and changed the 2×1 area nearby into a disordered structure. [S0163-1829(98)02824-0]

I. INTRODUCTION

In phase transitions at Si(111) and Ge(111) surfaces, steps and domain boundaries play leading roles. For example, at the cleaved Si(111) surface, 2×1 reconstruction with a π-bonded chain structure[1–6] changes irreversibly to 7×7 reconstruction in the annealing process at around 500 °C.[6–9] However, the manner of the transition depends on the distance from the nucleation sites, such as surface steps and domain boundaries.[8,9] Near the nucleation site, 2×1 first changes to a so-called ''1×1'' disorder phase. This ''1×1'' domain then changes to a 5×5 reconstruction. From small 5×5 domains near nucleation sites, 5×5 reconstruction extends over the surface, and finally 5×5 changes to a 7×7 reconstruction. The 7×7 reconstruction of the Si(111) surface also changes reversibly to the disordered structure (the so-called 1×1 phase) at around 830 °C.[10–15] Studies using a reflection electron microscope[11] and a low-energy electron microscope[12] have shown that the 7×7 reconstruction begins to nucleate at the top of the monoatomic steps on the Si(111) surfaces as the temperature is lowered. In the $c(2\times8)\leftrightarrow1\times1$ transition at the Ge(111) surface, the transition is initiated at the domain boundaries, and then extends over the entire surface.[13–15]

In these transitions, we observed that step edges and domain boundaries play special roles. This is due to their special atomic configurations. However, we found variety in the types of steps and domain boundaries, even on the same surface. We expected that the different types of steps or boundaries would play different roles in the transition. In this study, we investigated the $2\times1\rightarrow c(2\times8)$ irreversible transition on the cleaved Ge(111) surface, paying attention to the role of steps and domain boundaries of different types. The basic feature of this transition has been reported by Feenstra and Slavin.[6] On the Ge(111) surface, the 2×1 reconstruction changes to a $c(2\times8)$ reconstruction in the annealing process. During the transition, bilayer deep holes appear because the adatom density of $c(2\times8)$ exceeds that of the 2×1 reconstruction. The holes then disappear, and the $c(2\times8)$ reconstruction is completed. However, the cleaved Ge(111) surface has two types of boundaries and two types of step edges. The role of the different types of steps and boundaries has not been addressed in the transition. In the following, we show that the transition proceeds preferentially at a special type of step and boundary. Based on STM images, we discuss the atomic configuration and the reason for the activity of the special boundary and step in the transition.

II. EXPERIMENTAL APPARATUS

We cut the samples with dimensions of $7\times5\times0.2$ mm^3 from the *p*-type Ge(111) wafer. After introducing guiding grooves on both sides, we mounted the sample on the holder. This held the sample obliquely to expose its {111}-cleaved surface to the scanning tunneling microscopy (STM) tip. We then loaded the sample into the ultrahigh vacuum STM apparatus, consisting of the loading chamber, the preparation chamber with the cleavage mechanism, and the main chamber with the STM unit. The base pressure of the preparation and main chambers was less than 1×10^{-8} and 8×10^{-9} Pa. In the preparation chamber, we cleaved the sample by introducing a movable blade into one of the grooves. We transferred the cleaved sample into the main chamber, and observed its {111} cleaved cross section by STM. Details of our STM apparatus with the cleavage mechanism have been described elsewhere.[16,17]

The as-cleaved surface showed a 2×1 reconstruction. We heated the sample to cause the $2\times1\rightarrow c(2\times8)$ transition. We measured temperatures above 500 °C by an optical pyrometer. Below 500 °C, we estimated the temperature by interpolating the data of temperature vs heating current above 500 °C to the room temperature at zero current with the seventh-order polynomial. The polynomial connected the data from 500 to 1200 °C and room temperature smoothly

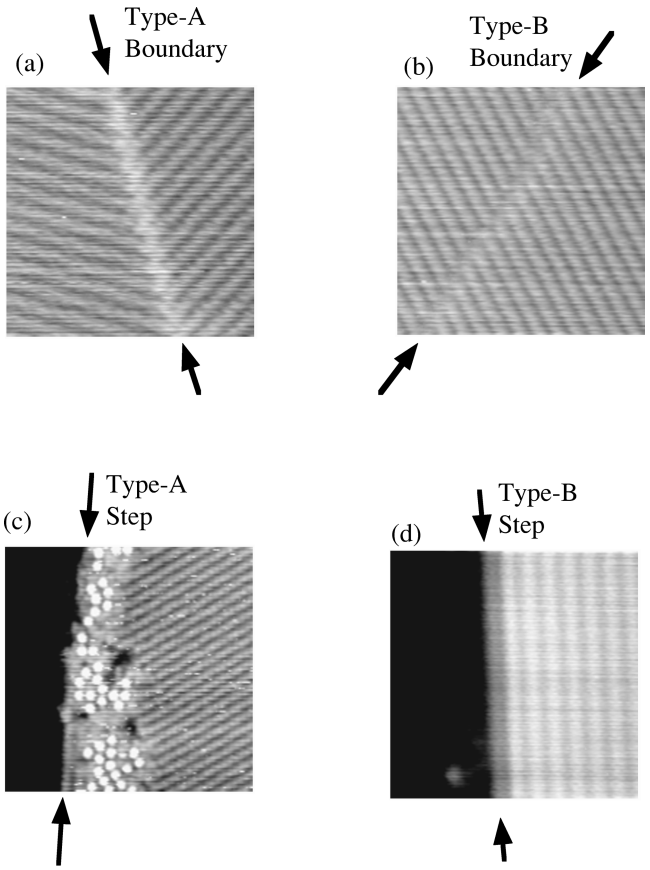

FIG. 1. STM images of the boundaries and steps at the cleaved Ge(111) surface. (a) Type-*A* boundary. 10×10 nm^2, -1.8 V, 0.3 nA. (b) Type-*B* boundary. 10×10 nm^2, $+2.0$ V, 0.3 nA. (c) Type-*A* step. 16×16 nm^2, $+1.7$ V, 0.7 nA. (d) Type-*B* step. 16×16 nm^2, $+1.3$ V, 0.2 nA. In all the figures, π-bond chains were imaged as bright lines. In (c) and (d), the lower terraces were imaged darkly. Only π-bond chains at upper terraces were imaged. All the π-bond chains are in the $\{\bar{1}10\}$ direction.

enough. Since the 2×1 to $c(2\times8)$ transition happens at temperatures which cannot be measured by the pyrometer, we estimated the temperature mentioned in this paper from the heating current by using the interpolated curve.

III. RESULTS

STM images of the as-cleaved $\{111\}$ surface are shown in Fig. 1. We observed the 2×1 reconstruction with the π-bonded chain structure.[6] Because of the threefold rotational symmetry of the surface, three 2×1 domains exist. We call the boundary [Fig. 1(a)] at which the direction of the π-bonded chains rotated to 120° the type-*A* boundary. Domains with the same direction as the π-bonded chains form an out-of-phase boundary (type-*B* boundary). At the type-*B* boundary, the π-bonded chains are staggered by a half-unit cell [Fig. 1(b)]. As with the domain boundaries, we call the step that is oblique to the π-bonded chains on the terrace a type-*A* step [Fig. 1(c)], and the step parallel to the π-bonded chains a type-*B* step [Fig. 1(d)]. As we observed in the figure, the type-*A* boundary and type-*A* step were found to be disordered locally, whereas the type-*B* boundary and type-*B* step were not disordered.

In the subsequent annealing, we found that the 2×1 reconstruction changed to a $c(2\times8)$ reconstruction via disordered phases. We studied the roles of the different types of boundaries and steps in the transition by STM images of the surface annealed at various temperatures. Results are shown in Fig. 2. We took each STM image at room temperature by quenching the surface after annealing for 5 min. The annealing temperatures are indicated in the figure. In the annealing process up to 100 °C, we noticed no change in the surface structure. The disordering began at the type-*A* boundary [Fig. 2(a)] and type-*A* step [Fig. 2(b)] at 120–130 °C. However, the type-*B* boundary [Fig. 2(b)] and type-*B* step [Fig. 2(a)] remained perfect. The disordering started from the type-*A* boundary and type-*A* step and extended into the 2×1 domains.

In the disordered area, we found adatoms arranged with 2×2 and $c(2\times4)$ short-range orderings. In addition, we frequently observed holes in the disordered area. Around these holes, some adatoms appeared grayish. Both the size and density of the holes were almost uniform in the disordered region; the average size of the holes was ~4 nm. We calculate that the holes occupied $\sim16\%$ of the disordered area. Between the holes, adatoms were arranged with short-range orderings. However, they never obtained $c(2\times8)$ long-range ordering in which the $c(2\times4)$ and 2×2 alternatively appear. In further annealings, the area of the disordered region increased. At 140 °C, the whole area of the surface changed to the disordered phase [Fig. 2(c)]. The holes increased in number, while their size and the density remained constant. Figure 3 shows the correlation of the annealing temperature to the area of the holes in the disordered region. As shown in the figure, below 140 °C, we found that $\sim16\%$ of the area was always occupied by holes in the disordered region.

At temperatures above 140 °C, the distinction between types *A* and *B* did not make sense because all of the π-bonded chain disappeared at the surface. At temperatures above 150 °C, the hole area in the disordered surface began to disappear (Fig. 3), and the adatom arrangement began to exhibit a $c(2\times8)$ long-range ordering. In our observation of the quenched surfaces, we recognized no evolution of the transition at the near-step region. In Fig. 2(d) of the 160 °C annealing, the small holes have almost disappeared, and have turned into large holes. At 170 °C [Fig. 2(e)], the large holes disappeared, and $c(2\times8)$ reconstruction appeared at some parts of the surface. The transition to the $c(2\times8)$ reconstruction was almost completed at 180 °C [Fig. 2(f)]. At temperatures above 190 °C, the surface changed to a $c(2\times8)$ reconstruction entirely.

IV. DISCUSSION

Initially, we discuss the stability of the type-*B* boundary against disordering. In the annealing process, the type-*A* boundary preferentially changed to the disordered phase, while the type-*B* did not change. We think that the stability of the type-*B* boundary is caused by its specific structure. Based on the high-resolution STM images of the boundary, we derive an atomic structure model for the type-*B* boundary as follows. The well-resolved, occupied STM image of the type-*B* boundary is shown in Fig. 4(a). The boundary crosses from upper left to lower right. Each atom of the π-bonded chains was imaged separately, which is useful in order to analyze the atomic structure of the type-*B* boundary. In the π-bonded chains, the atoms are buckled;[18,19] that is, the up-

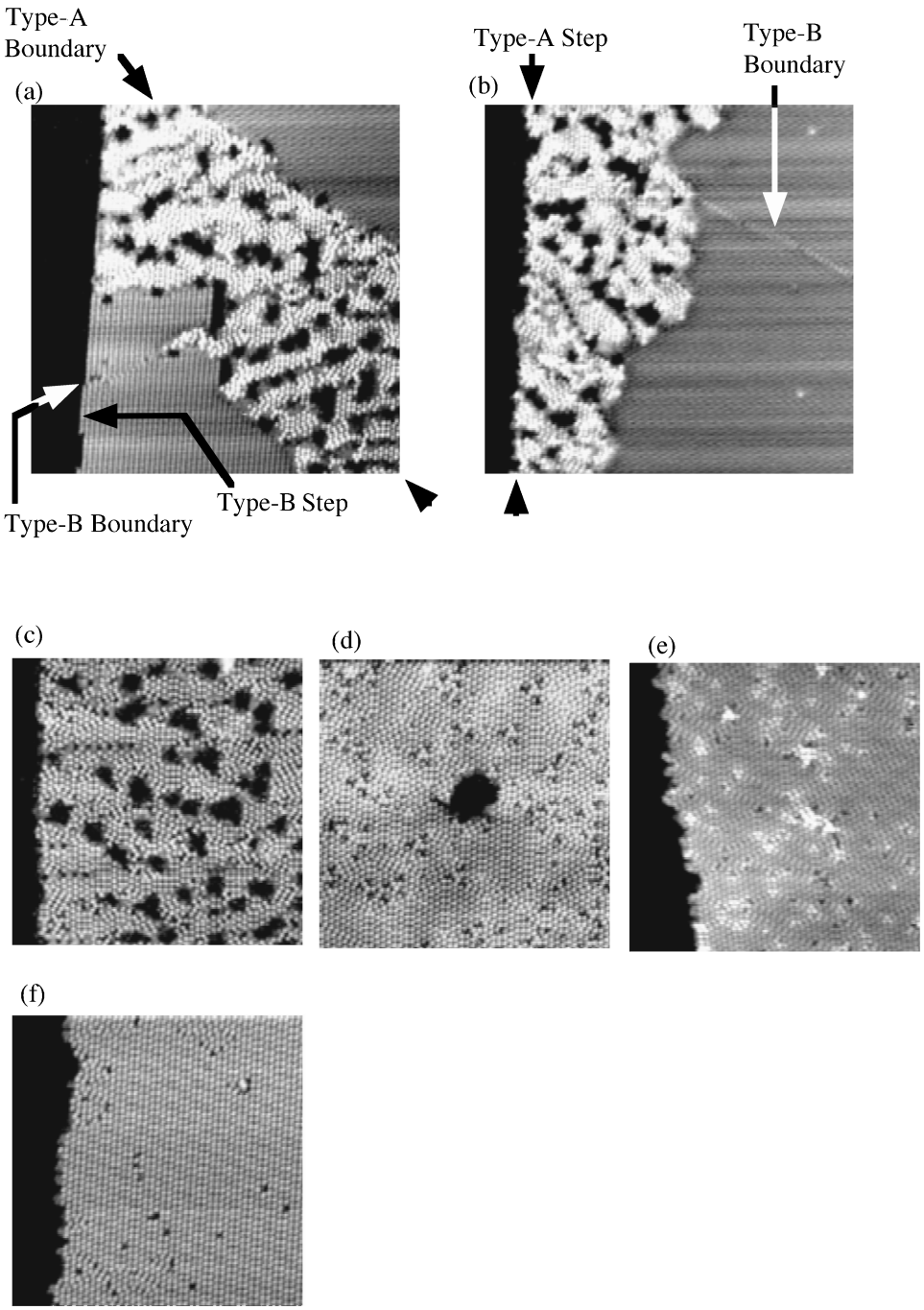

FIG. 2. The transition from 2×1 to $c(2\times8)$ reconstruction upon annealing. 47×47 nm^2. (a) At 130 °C. The disordering started from the type-*A* boundary, while the type-*B* step was not disordered. $V_s=+1.23$ V, $I_t=0.32$ nA. (b) At 130 °C. Disordering also started from the type-*A* step, while the type-*B* boundary was not disordered. $V_s=+1.23$ V, $I_t=0.32$ nA. (c) At 140 °C. The entire surface was covered by the disordered phase. $V_s=+2.00$ V, $I_t=0.30$ nA. (d) At 160 °C. Small holes in the disordered phase disappeared. Instead, a small number of large holes are generated. $V_s=+2.00$ V, $I_t=0.30$ nA. (e) At 170 °C. Large holes also disappeared. $V_s=+2.00$ V, $I_t=0.30$ nA. (f) At 180 °C. The $c(2\times8)$ reconstruction covered most of the surface. $V_s=+1.80$ V, $I_t=0.49$ nA.

per and lower atoms appear alternatively as illustrated in the side view of Fig. 4(b). The buckling makes the upper atom sp^3 coordinated, and the lower atom sp^2 coordinated.[19] The sp^3- coordinated atom has its dangling-bond state in midgap, whereas the sp^2-coordinated atom has its dangling bond state near the conduction band. In a detailed calculation,[18] the upper atom has more p-like character, which causes the lower shift of the dangling-bond state. Therefore, in the occupied STM image of Fig. 4(a), protrusions in π-bonded chains are due to dangling bonds at the upper atoms.

At the type-*B* boundary, the π-bonded chains are staggered by a half-unit cell. Thus we would expect that the

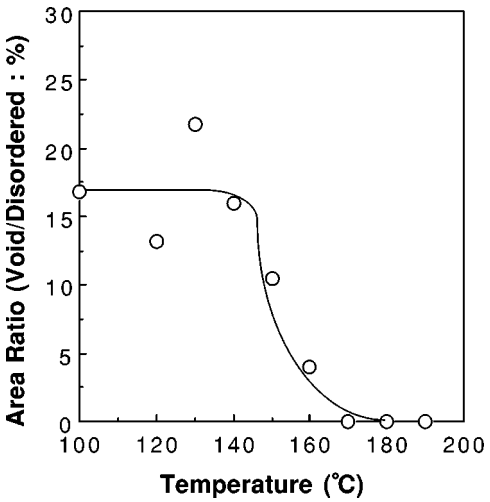

FIG. 3. Area ratio of holes in the disordered area. In the annealing below 140 °C, holes occupied ~16% of the disordered area. The area of the holes decreased rapidly at temperatures above 150 °C.

π-bonded chains would be disturbed around the boundary. However, judging from protrusions in the STM image, the π-bonded chain structure seems to remain even at the edge of the boundary. This suggests to us that the edge atoms have bondings similar to those of the atoms in the 2×1 domain. In the 2×1 domains, each atom of the π-bonded chains has two bonds to its neighboring atoms in the chain, and one bond to its neighboring atom under the chain (i.e., in the second bilayer). The atom under the chain has two bonds to its neighboring atoms in the second bilayer, one bond to its neighboring atom in the π-bonded chain, and one bond to the atom in the third bilayer. By these specific bondings of atoms in the π-bonded chain and in the second bilayer, the π-bonded chain structure is stabilized. At the type-*B* boundary, the edge atom of the π-bonded chain missed one of its two neighboring atoms of the chain because the π-bonded chain staggers by a half-unit cell. The edge atom in the second bilayer also missed one of its two neighboring atoms in the second bilayer for the same reason. In our model of the type-*B* boundary, the edge atom of the π-bonded chain makes a bond to the edge atom in the second bilayer of the other side [as indicated by the thick lines in Fig. 4(b)]. This bonding compensates atoms at the boundary for their lack of neighboring atoms. Moreover, this bonding enables the edge atoms take positions similar to those of the π-bonded chain, as illustrated in Fig. 4(b).

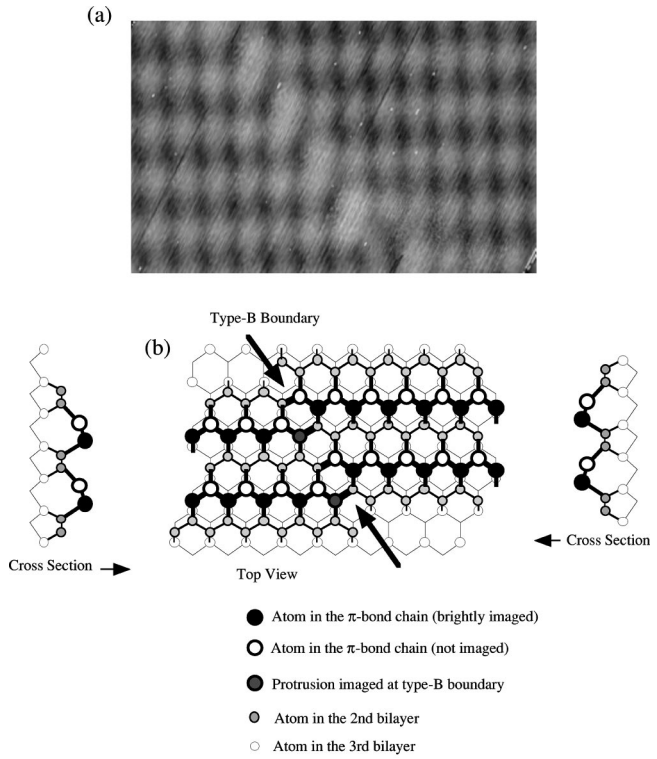

FIG. 4. Highly resolved, occupied-state STM image (a) and its model of the atomic arrangement (b) of the type-*B* boundary. The STM image was taken with $V_s=-1.00$ V, $I_t=0.50$ nA. In the occupied-state STM, the upper atoms in the π-bond chain caused protrusions as indicated by black circles in the figure (b). At the boundary, the atoms at the end of the upper line of the π-bond chains also caused these protrusions (indicated by the gray circle). The alignment of the black and gray circles agrees with the protrusions observed in occupied-state STM image.

We constructed the above atomic structure of the type-*B* boundary by using stick-and-ball models. Our proposed structure could be constructed without changing the length of the sticks (the bulk Si-Si bond length) for the edge atoms. Though back bonds became slightly flatter for the edge atoms of the π-bonded chain, the buckling remained even at the edge of the boundary. Therefore, in addition to the upper atoms (black circle) of the π-bonded chain, we expected the edge atoms in line with the upper atom (shaded circle) to be imaged as protrusions in the occupied-state STM image. In this assumption, our model agrees with the observed STM image. In the STM image [Fig. 4(a)], the protrusions align along the π-bonded chain with equal spacing to the edge of the boundary, and, at the boundary, the protrusion jumps to the off-normal (i.e., upper right) direction. It then connects to the half-staggered π-bonded chain in the counterpart domain. This agrees with the protrusion we expected for the occupied-state STM in our model [shaded and black circles in Fig. 4(b)]. Therefore, we believe that our model is realistic.

In our model, the π-bonded chains are bridged smoothly from one domain to another, in spite of the stagger, over the type-*B* boundary. Because of the bonding to the atoms in the second bilayer of the other side domain, the edge atom of the π-bonded chain has one dangling bond, as does the atom within the π-bonded chain. This also makes all bonds of the edge atom in the second bilayer saturated. Thus no additional dangling bond appears at the type-*B* boundary. As in the case of the type-*B* boundary, the 2×1 domains were smoothly connected at the type-*B* step edge. The atomic structure of the type-*B* step was reported for the Si(111)2×1 reconstruction by Feenstra and Stroscio.[20] Based on their detailed STM observation, they proposed models of the type-*B* step in which the 2×1 domain at the upper terrace is connected smoothly to the 2×1 domain at the lower terrace with natural bondings.

Contrary to the type-*B* boundary and type-*B* step, bondings are not smooth at the type-*A* boundary and type-*A* step. Since the π-bonded chains rotate at the type-*A* boundary, it is impossible to bond edge atoms over the boundary by way of our model for the type-*B* boundary. As a result, some bonds remain unsaturated at the type-*A* boundary. At the type-*A* step, the π-bonded chains are oblique to the step

edge. Therefore, it is equally impossible to take the bonding configurations as type-*B* step. This causes the appearance of unsaturated bonds of the π-bonded chains at the edge of the type-*A* step. The atom with unsaturated bonds is weakly bonded and easily released from the edge. Thus the type-*A* boundary and type-*A* step are unstable, in contrast to the type-*B* boundary and type-*B* step.

Upon annealing, atoms are released from the unstable edges of the π-bonded chains at the type-*A* boundary. This creates holes at the boundary and converts a 2×1 area nearby to the disordered phase, where adatoms are arranged with $c(2\times4)$ and 2×2 short-range orderings. Both the $c(2\times4)$ and 2×2 orderings have a greater atom density in the surface bilayers than the 2×1 reconstruction.[6] Thus it is reasonable that the transition from the 2×1 structure to the disordered structure creates holes.

When the disordering begins, the transition front of the disordered region becomes a new boundary. At this new boundary between the disordered region and the 2×1 domain, it is impossible to terminate the π-bonded chains smoothly. Thus the edges of π-bonded chains are also unstable at the new boundary, which continues to release atoms easily to the disordered phase. In addition, holes are created at the boundary, and the 2×1 area nearby becomes disordered. During the expansion of the disordered area, holes of a similar size are generated. The size of the hole is proportional to the number of atoms released, which changes the 2×1 structure to $c(2\times4)$ and 2×2 structures around the hole. Therefore, the increase in the number of the holes of constant small size indicates that the disordering proceeds by the expansion of the transition in small areas determined by diffusion. In this manner, the disordering extends from the type-*A* boundary and type-*A* step into the 2×1 domain.

The $c(2\times4)$ and 2×2 adatom arrangements in the disordered area have a 12.5% greater atom density in the surface bilayers than does the 2×1 reconstruction. However, the holes which appear in the disordered region are bilayer deep.[6] Thus the disordered area should include an 11% $[=12.5/(12.5+100)\%]$ hole area. In our experiment, the disordered region included holes of $\sim$16% during its extension. This agrees with the above expectation. After covering the whole surface, the area of the holes decreased at above 150 °C. A net increase in the number of surface atoms is necessary for this decrease of the hole area. We believe that the detachment of atoms from the step edges, which is thermally activated at this temperature, is the reason for the net increase in surface adatom density.

V. SUMMARY

We studied the transition from the 2×1 to the $c(2\times8)$ reconstruction on the Ge(111) cleaved surface by using STM. The cleaved surface showed a 2×1 reconstruction with π-bonded chains. At the 2×1 surface, type-*A* and -*B* domain boundaries appeared. Type-*A* step and -*B* steps also existed on the surface. Upon annealing, we found that the 2×1 reconstruction is preferentially disordered at the type-*A* boundary and type-*A* step. However, the type-*B* boundary and type-*B* step were stable against disordering. From the type-*A* boundary and type-*A* step, disordering extended into the 2×1 domains. Eventually, the disordered phase covered the whole surface.

On the basis of the high-resolution STM image, we proposed an atomic structure model for the type-*B* boundary. At the type-*B* boundary, the end atom of the π-bonded chain bonds to the atom in the second bilayer 2×1 domain of the other side. Because of this bonding, the end atom takes a position similar to that of atoms in the 2×1 domain. However, it is impossible to bridge two 2×1 domains at the type-*A* boundary. Thus the edge of the π-bonded chain is unstable at the type-*A* boundary. This makes the type-*A* boundary and type-*A* step release atoms easily into the 2×1 domain. This release of atoms creates holes at the boundary, and causes the nearby area to become disordered. At the resulting boundary between the disordered and 2×1 areas, the termination of the π-bond chains is also unstable, and atoms are easily released into the 2×1, domain and the creation of holes and disordering of the 2×1 area nearby are repeated. In this manner, the disordered area expands from the type-*A* boundary and type-*A* step into the 2×1 domain.

ACKNOWLEDGMENT

We would like to thank Dr. T. Tatsumi for supplying the Ge(111) wafers.

*Author to whom correspondence should be addressed.

[1] K. C. Pandey, Phys. Rev. Lett. **47**, 1913 (1981).
[2] R. M. Feenstra, W. A. Thompson, and A. P. Fein, Phys. Rev. Lett. **56**, 608 (1986).
[3] J. A. Strocio, R. M. Feenstra, and A. P. Fein, J. Vac. Sci. Technol. A **5**, 838 (1987).
[4] R. M. Feenstra, J. A. Strocio, and A. P. Fein, Surf. Sci. **181**, 295 (1987).
[5] J. A. Strocio, R. M. Feenstra, and A. P. Fein, Phys. Rev. Lett. **57**, 2579 (1986).
[6] R. M. Feenstra and A. J. Slavin, Surf. Sci. **251/252**, 401 (1991).
[7] J. J. Lander, G. W. Gobeli, and J. Morrison, J. Appl. Phys. **34**, 2298 (1963).
[8] R. M. Feenstra and M. A. Lutz, Phys. Rev. B **42**, 5391 (1990).
[9] R. M. Feenstra and M. A. Lutz, Surf. Sci. **243**, 151 (1991).
[10] P. A. Benett and M. B. Webb, Surf. Sci. **104**, 74 (1981).
[11] N. Osakabe, Y. Tanishiro, K. Yagi, and G. Honjo, Surf. Sci. **109**, 353 (1981).
[12] W. Telieps and E. Bauer, Surf. Sci. **162**, 163 (1985).
[13] R. M. Feenstra, A. J. Slavin, G. A. Held, and M. A. Lutz, Ultramicroscopy **42-44**, 33 (1992).
[14] R. M. Feenstra and G. A. Held, Physica D **66**, 43 (1993).
[15] R. M. Feenstra, A. J. Slavin, G. A. Held, and M. A. Lutz, Phys. Rev. Lett. **66**, 3257 (1991).
[16] H. Hirayama, Y. Einaga, M. Koike, and K. Takayanagi, Surf. Rev. Lett. (to be published).
[17] H. Hirayama, M. Koike, Y. Einaga, A. Shibata, and K. Takayanagi, Phys. Rev. B **55**, 1948 (1997).
[18] N. Takeuchi, A. Selloni, A. I. Shkrebtii, and E. Tosatti, Phys. Rev. B **44**, 13 611 (1991).
[19] J. E. Northrup and M. L. Cohen, Phys. Rev. B **27**, 6553 (1983).
[20] R. M. Feenstra and J. A. Stroscio, Phys. Rev. Lett. **59**, 2173 (1987).